Eur. Phys. J. A **12**, 479–486 (2001)

THE EUROPEAN PHYSICAL JOURNAL A

Dissipative and fluctuating effects in nuclear dynamics with a wavelet representation

V. de la Mota[a] and F. Sébille

Subatech, 4 rue A. Kastler, BP 20722 44307 Nantes Cedex 03, France

Received: 17 July 2001 / Revised version: 2 November 2001
Communicated by A. Molinari

Abstract. Transport phenomenon in nuclear matter is addressed with the DYWAN model, which is based on the projection methods of statistical physics and on the mathematical theory of wavelets. Strongly compressed representations of the nuclear systems are obtained with a description of the wave functions and their antisymmetrization. Fluctuation-dissipation effects are investigated in nuclear collisions at intermediate energies and comparisons with experimental data and semi-classical models are presented. The study of different observables shows that these effects are correctly described in Ar + Ag and Mo + Mo reactions at different beam energies.

PACS. 25.70.-z Low and intermediate energy heavy-ion reactions – 21.60.Gx Cluster models

1 Introduction

The interest of understanding the decay mechanisms in nuclear reactions at intermediate energies is well known. Indeed, they constitute an appropriate framework for studying the properties of hot and condensed nuclear matter and for extracting information on the nuclear equation of state. New experimental facilities made possible the evidence of physical processes in heavy-ion physics like multi-fragmentation, vaporization and collective flow. Nevertheless, the theoretical description of these processes is not satisfactory yet. Among the different models devoted to the description of heavy-ion collisions (HICs) are the statistical models [1,2]. However, at intermediate energies the dynamics should play a significant role since the experimental data result from very violent and far from equilibrium processes. Dynamical models have been developed in the '80s decade by extending the Time-Dependent Hartree-Fock (TDHF) mean-field description in order to incorporate two-body collisions [3–6]. In particular, semi-classical versions of the Extended-TDHF (ETDHF) model have been shown to well reproduce the mean behavior of nuclear systems [7,8]. These models encounter two main difficulties. On one side, when the excitation energies rise sufficiently (exceeding the binding energies per nucleon), the formation of intermediate mass fragments (IMFs) becomes predominant and their description is beyond the scope of these models. On the other side, when the excitation energy is lower and the dynamics is mainly governed by the mean field, quantum aspects are increasingly important. Some advances have recently been made in both directions. In semi-classical ETDHF models, density fluctuations have been introduced through stochastic approaches [9,10]. Some quantum aspects are taken into account by introducing explicitly the fermionic nature of nucleons and the symmetry properties of single-particle (s.p.) wave functions [11,12] in molecular models, improving the so-called QMD [13] version, which cannot correctly describe neither the mean field nor the antisymmetrisation. Nevertheless, fermionic dynamical methods suffer from high calculation costs, which makes their application to the study of massive systems very difficult. Moreover, it has been recently argued [14] that the difficulty to describe fragment emission in these models lies on the Gaussian nature of the s.p. wave functions.

In this work we present the results of a new approach, the DYWAN (DYnamical WAvelet in Nuclei) model [15] founded on the projection method of statistical mechanics and on the wavelet theory. It has been developed with the aim of improving the physical description of nuclear dynamics of ETDHF-like models by including quantum effects and density fluctuations, in a compact and fast numerical treatment of the representation space. In this paper, we will focus on the dissipation-fluctuation aspects in HICs, compared with experimental data. We will also discuss the advantages of the DYWAN model from a comparison with a semi-classical model. The next step would be the description of fragmentation processes, the results of which will be presented in a further paper. This work is organized as follows. In sect. 2 the theoretical basis of the model are presented. Section 3 is devoted to the description of the dissipative dynamics in Ar + Ag reactions at

[a] e-mail: delamota@subatech.in2p3.fr

27 and 44 MeV/n. In sect. 4 we address the description of Mo + Mo reactions at 18.7 MeV/n. In sect. 5 we present our conclusions and perspectives.

2 Bases of the model

The DYWAN model is based on the principles of projection methods [16], by which the description of a complex system, compatible with our incomplete knowledge of its state, is given in terms of the projection of the complete density matrix onto the subspace associated with the available information. In this sense a hierarchy of approximations can be built according with the level of complexity of the description. In the case we are concerned with, the nuclear dynamics at intermediate energies, these different levels are connected with the treatment of high-order multi-particle correlations. Indeed, at the lowest level, the description is given by the projection of the space of states onto the one-body subspace, neglecting all couplings with other degrees of freedom. This is the TDHF approximation where the dynamics is completely ruled by the mean-field, with no particle correlations. In a second level stands the Extended-TDHF description, where a coupling with two-particle correlations is kept in order to include dissipative effects. At this level, the mean field is still playing a preponderant role. Going beyond the ETDHF level would need to introduce higher-order particle correlations, but the degrees of freedom can be so numerous that the problem becomes intractable. In this paper we propose a simplified form for the treatment of dynamical multi-particle correlations, which are necessary for the description of density fluctuations and the dispersions of dynamical observables.

2.1 Dissipative dynamics

The dissipative evolution of the one-body density matrix is given by the ETDHF equation

$$i\dot{\rho} = [h(\rho), \rho] + iI(\rho)\,, \tag{1}$$

where $h(\rho)$ is the self-consistent one-body Hamiltonian and $I(\rho)$ is the collision term. Despite the strong assumptions made to derive this equation, it is still complex and needs an adequate numerical treatment. The wavelet theory provides a convenient mathematical background to develop a methodology for the resolution of the dynamical equations since it is based on the same concepts as the approximation schemes involved in the physical description [15].

Equation (1) is solved by expanding the restricted one-body space of states onto a basis of non stationary wavelets [17]. As shown in ref. [15] these functions are chosen in order to correctly reproduce the static properties of nuclei. The ground states of nuclei are prepared by performing a multi-resolution analysis [18] of the s.p. wave functions. The problem is self-consistent, starting from a set of trial s.p. wave functions, an iterative procedure is implemented in which the one-body density matrix and the self-consistent mean field are constructed from the analyzed wave functions. The s.p. wave functions φ^λ, associated with a nucleon level λ can be written as follows:

$$|\varphi^\lambda\rangle = \sum_i \omega_i^\lambda |\psi_i^\lambda\rangle\,, \tag{2}$$

where $\{\psi_i\}$ is an orthogonal wavelet basis and $\{\omega_i^\lambda\}$ are the corresponding weights.

In this description we choose for $\{\psi_i\}$ a spline basis [19]. As a matter of fact, the different families of wavelet bases present several interesting mathematical properties, and then they offer the opportunity to use bi-orthogonality and symmetries to extract efficiently the fundamental quantum properties of the analyzed functions. The one-body density matrix then reads

$$\rho = \sum_{\lambda=0}^{N} \sum_{i,j} \beta_{i,j}^\lambda |\psi_i^\lambda\rangle\langle\psi_j^\lambda| \tag{3}$$

with $\beta_{i,j}^\lambda = \omega_i^\lambda \omega_j^{\lambda *}$. As stated elsewhere [15] the advantage of the wavelet basis is its ability to concentrate the most relevant information on a reduced number of coefficients according to their spatial and frequential structure.

The wavelet decomposition provides the model with a natural link to the dynamical properties of the system. Indeed, any family of wavelets can be generated by the application of a given mathematical transformation on a reference function. Then, wavelets can be considered as a class of generalized coherent states, their group properties giving the framework of a reliable representation of the dynamics. Numerical solutions of the TDHF-like equations are found by means of a variational principle. In this work we use the fact that the spline wavelets can be analytically approximated by a linear combination of squeezed coherent states [20]. The motion of the system is then given in terms of the time evolution of the translation and dilation parameters of the projection basis [15]. It has been shown in ref. [15] that the variational principle provides a set of coupled differential equations for the time evolution of first and second moments in position and in momentum. The one-body wave functions are the solutions of the corresponding ETDHF equation compatible with eq. (1), while their occupation rates obey to a master equation [3], which accounts for the irreversible evolution towards equilibrium.

In this work we have implemented a very simplified effective force in the mean-field term of eq. (1), the Zamick force [21], in order to extract a first insight about the characteristics of the description given by the DYWAN model. The Hartree-Fock potential related to the Zamick interaction reads

$$V_{\rm HF}(\rho) = t_0\rho + t_3\ \rho^{\nu+1}\,, \tag{4}$$

where ρ is the local density, and t_0, t_3 and ν are parameters adjusted to give saturation properties of infinite symmetric nuclear matter, with $t_0 = -356\,\mathrm{MeV}/\rho_\infty$,

$t_3 = 303\,\mathrm{MeV}/\rho_\infty{}^{\frac{7}{6}}$, $\nu = \frac{1}{6}$. In particular, the saturation density value is $\rho_\infty = 0.145$ fm^{-3} and the incompressibility modulus is $K_\infty = 200$ MeV.

On the other side, the nucleon-nucleon cross-section in the master equation is the free one, energy and isospin dependent without in-medium corrections.

2.2 Many-body information

In order to describe fragment production and the dispersions of observables in heavy-ion reactions, theoretical models must go beyond the one-body level. As stated before, a fully microscopic treatment of multi-particle correlations, involved in N-body dynamics, is in practice untractable. In this section we address a method to treat the many-body information about the system from a statistical point of view.

At any time, the many-body system can be represented by a linear combination of Slater determinants of single-particle wave functions:

$$|\Psi^N\rangle = \sum_K a_K(t)|\Phi_K^{(N)}\rangle\,, \tag{5}$$

$$|\Phi_K^{(N)}\rangle = A[|\varphi_1\rangle, .., |\varphi_a\rangle]\,, \tag{6}$$

where A is the antisymmetrization operator and the $\{\varphi_i\}$ are the solutions of the ETDHF equation. The N-body density operator can therefore be written as

$$\rho^N(t) = \sum_{K,K'} a_K(t)a^*_{K'}(t)\ |\Phi_K^{(N)}\rangle\langle\Phi_{K'}^{(N)}|\,. \tag{7}$$

This expression is extremely detailed, but we can make the assumption that all off diagonal terms in ρ^N are rapidly oscillating and that their global contribution is, in average, negligible. Then, in such a random phase approximation, the N-body density matrix reads

$$D^N(t) = \sum_K |a_K(t)|^2\ |\Phi_K^{(N)}\rangle\langle\Phi_K^{(N)}|\,, \tag{8}$$

the coefficients $|a_K(t)|^2$ representing the statistical weights of the different Slater determinants. According to sect. 2, each s.p. wave function belonging to an individual Slater determinant is projected on a basis of wavelets (eq. (2)). The resulting approximated N-body density matrix is then given by the following expression:

$$D^N(t) = \sum_K |a_K(t)|^2 \sum_{M,M'} b_M b^*_{M'}|\Theta_M\rangle\langle\Theta_{M'}|\,. \tag{9}$$

Here, $|\Theta_M\rangle$ is a Slater determinant of wavelets, $b_M = \det(c^i_\lambda)$ and the c^i_λ are the coefficients of the decomposition of s.p. wave functions on the wavelets basis.

In this work, for computational reasons, we have made supplementary simplifications. We choose the weights of the different Slater determinants of wavelets uniformly distributed. This is consistent with a maximum entropy condition, and we kept only the diagonal contribution: terms with $M = M'$ in eq. (9). Nevertheless, if necessary, non diagonal terms can be calculated and restored at any time in this description. The N-body density matrix can then be represented as a superposition of Slater determinants of wavelets.

In this way, the many-body description given by this prescription is the least biased one, compatible with the dissipative one-body available information. Projecting eq. (9) on the one-body subspace we retrieve the wavelet expansion of the corresponding density matrix, ρ, which is the solution of the ETDHF equation (1). The initial expansion of the statistical N-body density matrix in terms of wavelets is obtained from the self-consistent treatment of the statics. All along the time evolution, the statistical weights evolve with the time dependence of the occupation numbers ruled by the master equation. Then Slater determinants are populated or de-populated according with the 2p-2h transitions involved in the collision term of eq. (1). In this statistical framework, fluctuations around the mean behavior, described by ρ, result from the contribution of each individual Salter determinant. These fluctuations are responsible of the widths in physical observables. In sect. 4 we show a particular application of this method for the description of the dispersions for a one-body observable, compared with experimental data.

3 Dissipation in ^{40}Ar + ^{107}Ag dynamics

A certain number of experiments have been performed in order to investigate the stability limits of excited nuclei. Among these experiments there exists an important amount of data in $^{40}\mathrm{Ar} + {}^{107}\mathrm{Ag}$ reactions performed at Ganil. In this section we will investigate the characteristics of particle spectra, temperature parameters and the correlations of different quantities in $^{40}\mathrm{Ar} + {}^{107}\mathrm{Ag}$ collisions at 27 and 44 Mev/n of incident energy with the DYWAN model. The impact parameter is chosen in the range $6\,\mathrm{fm} \leq b \leq 10\,\mathrm{fm}$ in order to eliminate fusion events. The dissipative evolution given by our model will be confronted with the experimental yields [22], and with the semi-classical Landau-Vlasov model (LV) which has been shown to provide a good description of the global thermalisation process in those reactions [23]. Two fragments, target- and projectile-like fragments have been detected experimentally in coincidences. In fig. 1 their relative velocity V_{rel} is displayed as a function of the emission angle of the light partner, Θ_{LF}, for the concerned energies. Here V_{p} and V_{C} stand for projectile and Coulomb velocities. The ratio $(V_{\mathrm{rel}} - V_{\mathrm{C}})/(V_{\mathrm{p}} - V_{\mathrm{C}})$ tends towards zero for the most damped collisions, *i.e.* for the largest values of Θ_{LF}. The experimental data are represented by stars, while calculations with LV model are in diamonds and triangles, and those of the DYWAN model are in squares. In both models the nucleon-nucleon cross-section σ_{nn} is energy and isospin dependent without in-medium corrections.

It can be observed that the LV results globally overestimate the experimental data at 27 MeV/n and underestimate them at 44 MeV/n, while the DYWAN approach exhibits results closer to the experimental ones at both

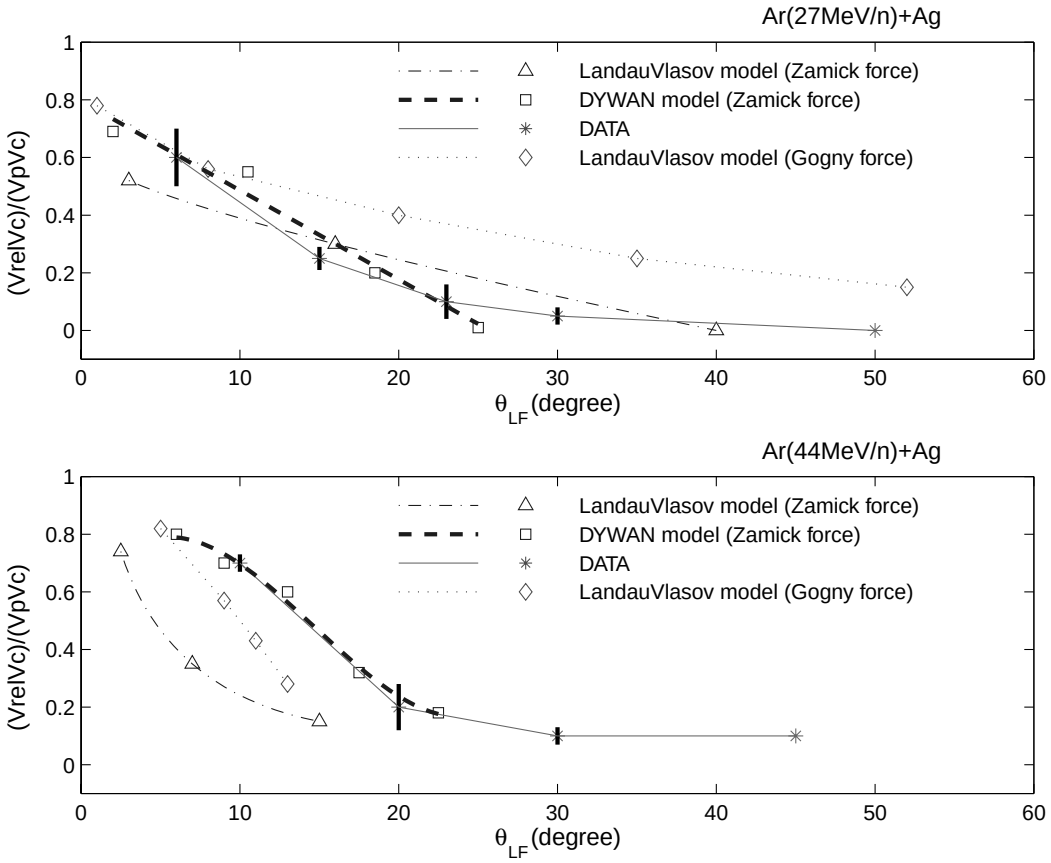

Fig. 1. Relative velocities as a function of the light-fragment angle in Ar + Ag reactions at 27 MeV/n (top) and 44 MeV/n (bottom).

incident energies. It must be underlined that the Zamick effective interaction [21] is a zero-range Skyrme-type force, while the Gogny force is non local. In the exit channel of the collision the relative velocity of the two remnants results from the dissipative effects generated by the residual interactions. The deflection of the light fragment is due to a competition of the repulsive and attractive components of the mean field, the kinetic pressure and the Coulomb repulsion. At these incident energies, and with the range of impact parameters involved, the action of the attractive part of the self-consistent potential is predominant. Comparing DYWAN results (squares) with LV ones (triangles) at 44 MeV/n we observe that, for a given amount of dissipation, the deflection is more important in the first case than in the second one. This enhancement in the DYWAN model is related to the spreading of the wave functions in the overlap zone of the two impinging nuclei. This spreading is illustrated in fig. 15 in ref. [15], it acts to enforce the attractive part of the nuclear potential providing greater scattering angles of the light fragment. The consequences on the density distribution of the colliding system are shown in fig. 17 of ref. [15]. In comparison with LV model, a stronger anisotropy appears in the density profiles along the axis joining the two partners of the binary system during the more violent stage of the collision. The self-consistent mean field will act afterwards, making the outgoing fragment more homogeneous and isotropic. On the contrary, this effect is practically not observed at the lower incident energy, where the process is slower in both descriptions. As a matter of fact, the self-consistent mean field has enough time to reorganize the densities towards more homogeneous and isotropic distributions. Therefore the results for both models are very similar. The general trend of LV calculations with the Gogny force (diamonds) is to provide greater relative velocities. In the peculiar case of the observables studied here, the non locality of the nuclear interaction leads to a lower damping of the relative motion. This effect is mainly due to the resulting effective masses of nucleons, which weaken the action of the residual interactions [7].

Despite an overall good agreement with experimental data, let us stress that it cannot be argued that the DYWAN model with a Zamick force provides the correct description of experiments. Nevertheless, this underlines that the quantum structure of the colliding system has to be taken into account, in order to investigate properly refined physical aspects, like those related to in-medium effects. Concerning these effects, the previous results support the conclusions of ref. [23].

Another interesting correlation is the recoil velocity $V_{\rm rec}$ of the binary system, before it breaks in two fragments, as a function of the light-fragment deflection.

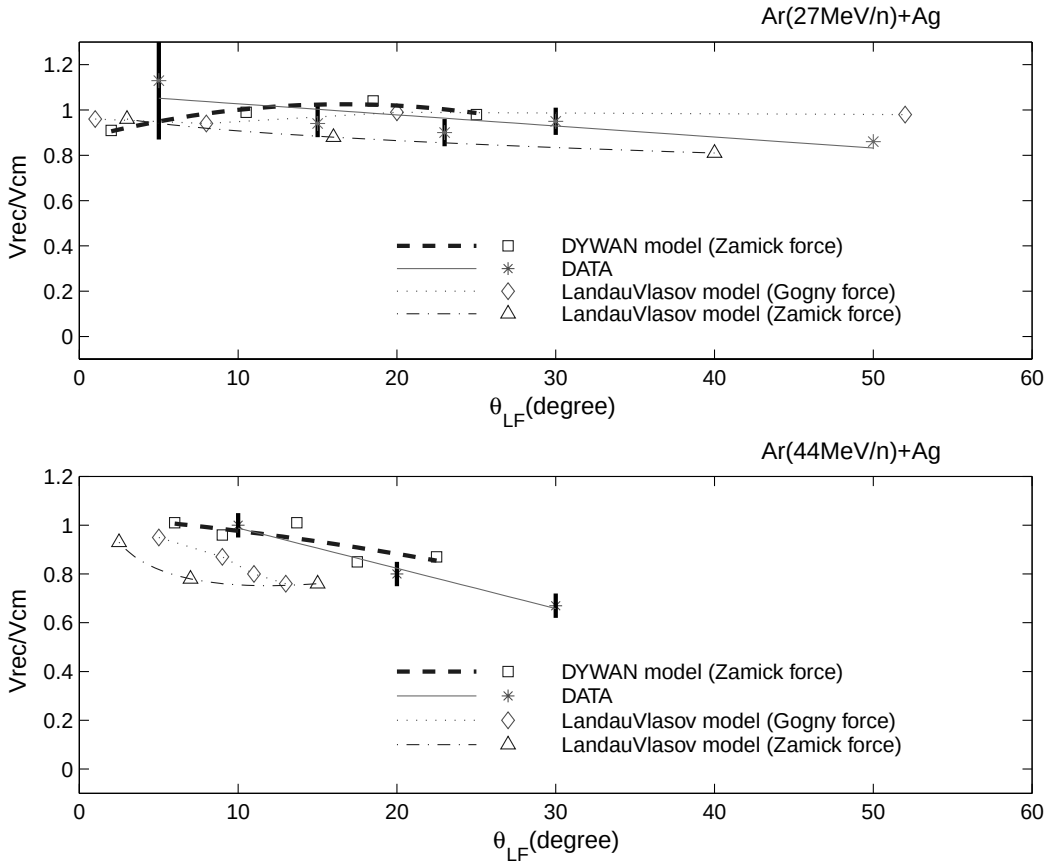

Fig. 2. Normalized recoil velocity of heavy fragments as a function of the light-fragment angle in Ar + Ag reactions at 27 MeV/n (top) and 44 MeV/n (bottom).

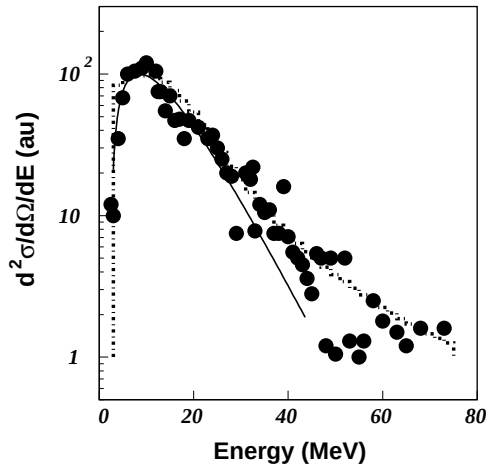

Fig. 3. Double differential emission spectra in Ar + Ag collisions, at 27 MeV/n. Full circles correspond to the experimental data from ref. [24], the dash-dotted line to DYWAN calculations.

Indeed, it allows to characterize the pre-equilibrium emission in a simple way [23], since the quantity $V_{\rm rec}/V_{\rm CM}$ is less than 1 if there is a dominant pre-equilibrium emission. In fig. 2 is depicted $V_{\rm rec}/V_{\rm CM}$ *versus* $\Theta_{\rm LF}$, where $V_{\rm CM}$ is the center-of-mass velocity of the initial system for the same energies and the same theoretical calculations as in fig. 1. Both models reproduce the global trends: a growing importance of the pre-equilibrium emission with the violence of the collision. For the two models the agreement with the data is good. Nevertheless, at the higher energy, they are slightly underestimated by the LV model. In both pictures we can observe that for angles $\Theta_{\rm LF} \sim 25°$ and higher there are no yields with the DYWAN model. This is due to the fact that, in these calculations, there are no binary processes in the case of the most central collisions. On the contrary, in LV calculations a light fragment can be found even at large angles. Despite the fact that the observable we are dealing with in fig. 2 addresses a different aspect of the dynamics, as the pre-equilibrium emission, the results support the same arguments as in the discussion of fig. 1. The recoil velocity can be considered as a global measure of the pre-equilibrium emission and it undergoes the same range of values for identical nuclear interactions.The differences between the models appear at the higher incident energy. They are evidenced by the deflection of light fragments, which bears the fingerprints of the wave functions spreading in the DYWAN model.

The experimental double differential cross-section $\mathrm{d}^2N/\mathrm{d}E\mathrm{d}\Omega$ from ref. [24] (full circles), together with the results of our calculations (dashed-dotted line) are displayed in fig. 3. The full line is extracted from a fitting of

Table 1. Apparent temperatures at two energies for different centralities with LV and DYWAN models compared with experiment.

$E/A = 27\,\mathrm{MeV}$	$V_{\mathrm{hf}} < 1\,\mathrm{cm/ns}$	$1 < V_{\mathrm{hf}} < 1.6\,\mathrm{cm/ns}$	$V_{\mathrm{hf}} > 1.6\,\mathrm{cm/ns}$
T_{app} (MeV) experiment	5.5	6.0	6.1
T_{app} (MeV) DYWAN	5.5	5.5	6.0
T_{app} (MeV) LV	7.2	6.8	6.8
$E/A = 44\,\mathrm{MeV}$	$V_{\mathrm{hf}} < 1\,\mathrm{cm/ns}$	$1 < V_{\mathrm{hf}} < 1.6\,\mathrm{cm/ns}$	$V_{\mathrm{hf}} > 1.6\,\mathrm{cm/ns}$
T_{app} (MeV) experiment	5.5	5.5	7.0
T_{app} (MeV) DYWAN	5.5	6.5	7.0
T_{app} (MeV) LV	7.2	6.5	

the experimental cross-section with the Weiskopf function [23]. The general trends, as the shape and the location of maxima, are pretty well reproduced. The characteristics of spectra are in agreement with the experiment over several orders of magnitude. This is not the case in semi-classical models where the agreement with the data is at most of two orders of magnitude. This aspect is connected with the fact that these models use a Gaussian sampling of the phase space giving a semi-classical distribution function which is much less homogeneous in phase space than with the wavelet basis.

The apparent temperatures were also estimated, according with the Weisskopf parameterization. In table 1 we can compare the temperatures calculated with DYWAN and LV models for two different energies. The experimental results [22] have also been reported for the same energies. As in experiment, events were sorted out in terms of centrality, which is estimated with the velocity of the heavy fragment V_{hf}. Three different ranges of centralities have been then considered. We see that the results obtained with the DYWAN model follow the experimental trends: temperatures increasing with the centrality of the collision. With the semi-classical LV model temperatures are rather independent of the characteristics of the reaction (energy and impact parameter). The main difference between both results can be found in the way in which the energy is deposited for both descriptions. Indeed, in the former, the collisions are treated quantum mechanically through the transitions of the colliding wavelets between the concerned s.p. levels. In this case the individual transitions affect the whole system, shearing the energy in a more efficient way than in the semi-classical model. In the latter, collisions are treated in a local approximation and take place mainly in the overlap region. This aspect explains its insensitivity to the centrality and to the energy of the reaction. The LV model gives apparent temperatures which are systematically higher than the experimental ones, it stems from the phase space sampling which cannot ensure an accurate account of the Pauli blocking.

4 Fluctuations in ^{100}Mo + ^{100}Mo reaction

The ^{100}Mo + ^{100}Mo reaction at 18.7 MeV/n has been performed at GSI laboratory. In this reaction the prompt binary fission taking place after an incomplete fusion is one

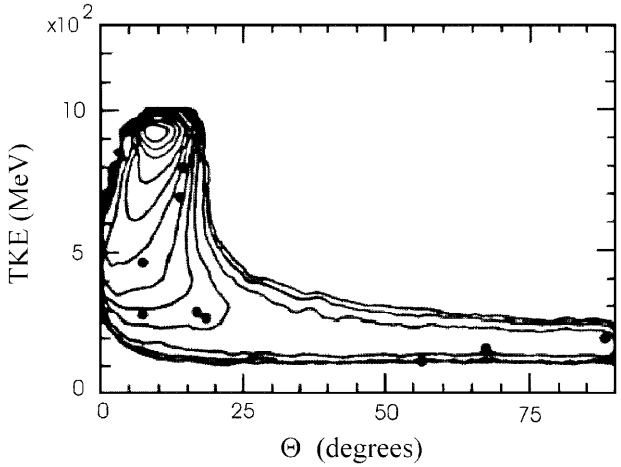

Fig. 4. Experimental Wilczynski plot in Mo + Mo reaction at $E/A = 18.7\,\mathrm{MeV}$.

of the most probable decay channels [25]. A typical characterization of this kind of reactions was given by Wilczynski plot in which the total kinetic energy (TKE) of the fragments is displayed as a function of the scattering angle in the center-of-mass frame. In ref. [26] a simulation with the LV model was compared with the experimental results, the ability of this semi-classical model to reproduce the mean trends has been shown. Nevertheless, this kind of model is unable to describe the dispersions of observables around their mean values. In fig. 4 LV mean values, obtained with the Zamick force (eq. (4)), are represented by full dots, superposed to the experimental values from ref. [25]. Each point corresponds to a given value of the impact parameter. According with the experiment, only binary events have been considered in the calculation. In fig. 5 we represent the Wilczynski plot calculated in the framework of the DYWAN model with the same Zamick force. The dispersions in the TKE values were treated as described in sect. 2 for a sampling of 1000 Slater determinants per impact parameter. Only a crude sampling of impact parameters has been made, with an average step value of 1 fm. The theoretical results were not corrected to take into account the details of experimental biases and a refined comparison with experiment was not addressed. Comparing figs. 4 and 5, the levels of the contour plots are not identical, the theoretical ones were built according to

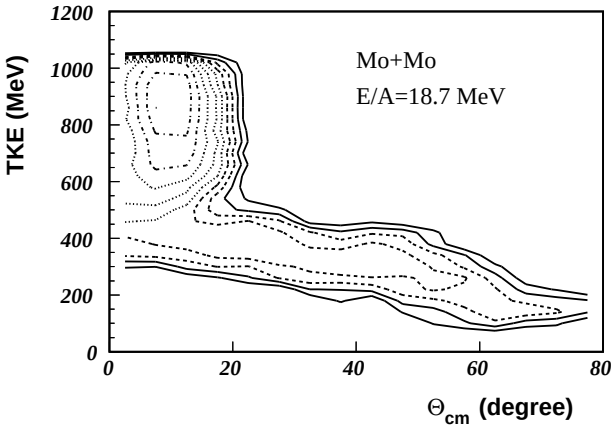

Fig. 5. Total kinetic energy as a function of the scattering angle in the center-of-mass frame in Mo + Mo at 18.7 MeV/n, calculated with the DYWAN model.

a logarithmic scale which follows approximately the experimental scaling. Nevertheless, the global dispersion in the diagram is in agreement with the experiment. The mean values are also correctly located, in particular, we find the Coulomb deflection in very peripheral reactions at around 1000 MeV as expected. For semi-peripheral and peripheral events the trajectories exhibit small deflections, which result from a competition between the mean field and the Coulomb repulsion. In the case of more central events the scattering angles cover all the angular range between 0 and 80 degrees, the TKE values lying around the Coulomb repulsion. The general shape of the Wilczynski plot is well reproduced, in particular it gives the correct localization in TKE of the transition from negative to positive deflections. Nevertheless, some differences appear at small angles for TKE values around 200 MeV. This difference is due to the already-mentioned coarse sampling in impact parameters. A noticeable difference between LV and DYWAN results appears in the most peripheral reactions. In this case, LV yields deviate from the "maximum" experimental ones, which are better reproduced by DYWAN calculations. This behavior also stems from the previously discussed quantum effects related to the spreading of the wave function. It contributes to negative deflections while the Coulomb repulsion to the positive ones. The balance between both effects gives the observed deflection.

5 Conclusions

In this work we have presented theoretical calculations in heavy-ion collisions at intermediate energies with the DYWAN model. These results have been compared with experiments and with the semi-classical Landau-Vlasov (LV) transport model. A novel approach to address the fluctuations of observables around their mean values has been proposed. It is based on a statistical assumption for the N-body description, in which the least biased many-body density matrix is given by a statistical mixture of Slater determinants of wavelets. Firstly, we showed that the DYWAN model gives the expected dissipative behaviors observed in heavy-ion collisions at those energies, this has been evidenced in the analysis of complementary observables in Ar on Ag collisions at 27 and 44 MeV/n. Secondly, we have also studied Mo + Mo reaction and investigated the dispersions in the correlation between the total kinetic energy (TKE) and the scattering angle in the center-of-mass frame. The results of DYWAN simulations are in good agreement with the experimental data. Differences appear with the semi-classical LV model, in particular, in the impact parameters ranges involved in both simulations. For a given TKE value the LV results are obtained for more central collisions than in DYWAN calculations. These differences are connected with the ability of these two models to take into account the quantum structure of the nuclear system, which are related to two main aspects. One of them is the description of the system in terms of wave functions, the other one is connected to the antisymmetrization for the Pauli-blocking term. The previous results with the DYWAN model are very encouraging, since even with a simple local effective force they confirm the expected behavior of the average values of observables, and at the same time they permit to correctly reproduce their dispersions. In consequence, they give the opportunity to address more refined aspects as the implementation of in-medium corrections and of a momentum-dependent effective force, like the Gogny force. We stress the fact that the model provides a well-defined N-body information related to the fluctuation-dissipation effects in the nuclear dynamics. In this framework, the study of fragment formation in heavy-ion collisions at intermediate energies can be undertaken and it is now in progress.

References

1. J.P. Bondorf, A.S. Botvina, A.S. Iljinov, I.N. Mishustin, K. Sneppen, Phys. Rep. **257**, 133 (1995).
2. D.H.E. Gross, Rep. Prog. Phys. **53**, 605 (1990).
3. C.-Y. Wong, H.H.K. Tang, Phys. Rev. C **20**, 1419 (1979).
4. G.F. Bertsch, H. Kruse, S. Das Gupta, Phys. Rev. C **29**, 673 (1984).
5. C. Grégoire, B. Remaud, F. Sébille, L. Vinet, Y. Raffray, Nucl. Phys. A **585**, 317 (1987); P. Schuck, R.W. Hasse, J. Jaenicke, C. Grégoire, B. Remaud, F. Sébille, E. Suraud, Prog. Part. Nucl. Phys. **22**, 181 (1989).
6. A. Bonasera, F. Gulminelli, J. Molitoris, Phys. Rep. **243**, 1 (1995).
7. V. de la Mota, F. Sébille, B. Remaud, P. Schuck, Z. Phys. A **343**, 417(1992); B. Jouault, V. de la Mota, F. Sébille, G. Royer, F. Lecolley, Nucl. Phys. A **597**, 136 (1996).
8. C. Gale, G. Bertsch, S. Das Gupta, Phys. Rev. C **35**, 1666 (1987); A. Bonasera, G.F. Burgio, M. Di Toro, Phys. Lett. B **221** 233 (1989).
9. S. Ayik, C. Grégoire, Nucl. Phys. A **513**, 187 (1990).
10. J. Randrup, B. Remaud, Nucl. Phys. A **514**, 339 (1990).
11. H. Feldmeier, Nucl. Phys. A **428**, 147 (1990).
12. A. Ono, H. Horiuchi, T. Maruyama, A. Onishi, Prog. Theor. Phys. **87**, 1185 (1992).
13. J. Aichelin, Phys. Rep. **202**, 233 (1991).

14. K. Kiderlen, P. Danielewicz, Nucl. Phys. A **620**, 346 (1997).
15. B. Jouault, F. Sébille, V. de la Mota, Nucl. Phys. A **628**, 119 (1998).
16. R. Balian, Y. Alhassid, H. Reinhardt, Phys. Rep. **131**, 1 (1986).
17. A. Grossmann, J. Morlet, T. Paul, Ann. Inst. H. Poincaré **45**, 293 (1986).
18. I. Daubechies, *Ten Lectures on Wavelets* (AMS, Providence, 1992).
19. M. Unser, in *Wavelets: A Tutorial in Theory*, edited by C.K. Chui (Academic Press, 1992).
20. A.M. Perelomov, *Generalized Coherent States and their Applications* (Springer Verlag, 1986).
21. L. Zamick, Phys. Lett. B **45**, 313 (1973).
22. D. Jouan, B. Borderie, M.F. Rivet, C. Cabot, H. Fuchs, H. Gauvin, C. Grégoire, F. Hanappe, D. Gardes, M. Montoya, B. Remaud, F. Sébille, Z. Phys. A **340**, 63 (1991); M.F. Rivet et al., *Proceedings of the XXXI International Winter Meeting on Nuclear Physics, Bormio, 1993* (Ricerca Scientifica ed Educazione Permanente, Milano, 1993) p. 92.
23. F. Haddad, B. Borderie, V. de la Mota, M.F. Rivet, F. Sébille, B. Jouault, Z. Phys. A **354**, 321 (1996).
24. E. Vient et al., Nucl. Phys. A **571**, 588 (1994).
25. R.J. Charity et al. Z. Phys. A **341**, 53 (1991).
26. F. Haddad, G. Royer, F. Sébille, B. Remaud, Nucl. Phys. A **572**, 459 (1994).